SCIENTIFIC REPORTS

OPEN

SUBJECT AREAS:
CLIMATE-CHANGE IMPACTS
ATTRIBUTION
PHYSICAL OCEANOGRAPHY
ATMOSPHERIC DYNAMICS

Received
18 March 2013

Accepted
4 June 2013

Published
20 June 2013

Correspondence and requests for materials should be addressed to W.J.C. (Wenju.Cai@csiro.au)

Climate-change impact on the 20th-century relationship between the Southern Annular Mode and global mean temperature

Guojian Wang[1,2] & Wenju Cai[1]

[1]CSIRO Marine and Atmospheric Research, Aspendale, Victoria, Australia, [2]College of Physical and Environmental Oceanography, Ocean University of China, Qingdao, China.

The positive phase of the El Niño-Southern Oscillation (ENSO) increases global mean temperature, and contributes to a negative phase of the Southern Annular Mode (SAM), the dominant mode of climate variability in the Southern Hemisphere. This interannual relationship of a high global mean temperature associated with a negative SAM, however, is opposite to the relationship between their trends under greenhouse warming. We show that over much of the 20th century this relationship undergoes multidecadal fluctuations depending on the intensity of ENSO. During the period 1925–1955, subdued ENSO activities weakened the relationship. However, a similar weakening has occurred since the late 1970s despite the strong ENSO. We demonstrate that this recent weakening is induced by climate change in the Southern Hemisphere. Our result highlights a rare situation in which climate change signals emerge against an opposing property of interannual variability, underscoring the robustness of the recent climate change.

The SAM[1,2], also known as the Antarctic Oscillation[3] and high-latitude mode[4], is the dominant pattern of large-scale variability in the extratropical Southern Hemisphere. It describes large-scale alternations of atmospheric mass between the mid latitudes and high latitudes. In its positive phase, the SAM is associated with a higher-than-normal mean sea level pressure (MSLP) in mid latitudes and lower MSLP in high latitudes. The SAM also refers to a zonally symmetric north–south movement of the westerly belt that circles Antarctica. There is a southward shift of this belt during a positive phase of the SAM[2,5,6].

Variability of the SAM on an interannual time scale has been shown to be at least in part related to ENSO during the austral summer[7–17]. In particular, circulation anomalies associated with ENSO can force a significant part of the low-frequency variability, with a negative SAM being associated with an El Niño, and vice-versa. As an El Niño causes a higher global mean temperature (GMT), a negative SAM is also associated with a higher GMT on interannual time scales.

Over the past several decades Antarctic ozone depletion and emissions of greenhouse gases have been forcing a positive trend of the SAM[2,18], as GMT trends up. This is supported by simulations forced by greenhouse gases only[19–22] and by ozone depletion only[22–24]. Further, models with a greater warming trend tend to generate a greater SAM trend[25], with strengthening westerlies in the high latitudes but weakening westerlies in the mid latitudes[21]. The associated strengthening in mid-latitude wind stress curls, with a poleward shift of the zero-curl line, leads to a poleward shift of the Southern Hemisphere supergyre circulation[26,27], which links all the three subtropical gyres of the Southern Hemisphere. The long-term SAM trend is generated by climate change-induced enhancement in meridional temperature gradients in the stratosphere[23,28] and in the surface ocean[21,29].

The relationship between the long-term GMT trend and the SAM trend is therefore opposite to the interannual relationship, meaning that the long-term SAM trend emerges in spite of the opposing effect of interannual variability and does not project onto it, as is often suggested[30]. Here we investigate how stable the interannual GMT-SAM relationship is, assess the impact of global warming on the interannual relationship, and discuss the implication for climate change detection in the Southern Hemisphere, focusing on austral summer (December, January, and February, or DJF).

Results

Linkage between trends of increasing GMT and positive SAM under greenhouse warming. There are many studies documenting the global warming trend and the upward trend of the SAM over the past decades[2,18,26–28]. This linkage is even more conspicuous in realizations of simulated future climate, when these trends intensify, as produced by climate models contributing to CMIP3[31] and CMIP5[32] (see Supplementary Table S1 online). To illustrate this, we calculate the DJF GMT trends over the 2006–2099 period in each of the 31 available models ($GMT_{trend}(L)$, $L = 1, 31$, *representing models*), the SAM trends ($SAM_{trend}(L)$, $L = 1, 31$), grid-point zonal wind stress trends ($TAUU_{trend}(x, y, L)$, $L = 1, 31$), and grid-point wind stress curl trends ($CURL_{trend}(x, y, L)$, $L = 1, 31$), which provide a gauge of the associated ocean circulation changes[33]. A map of regression of $TAUU_{trend}(x, y, L)$ onto $GMT_{trend}(L)$, with respect to models (L) (Fig. 1a), yields a pattern similar to one associated with the SAM, reflecting that a positive GMT trend is associated with a positive SAM trend. Models with a larger GMT trend tend to produce decreasing westerlies in the mid latitudes and enhanced westerlies to the south.

The associated mid-latitude wind stress curl trends increase with GMT trends. This is indicated in Fig. 1b, which shows a map of regression of $CURL_{trend}(x, y, L)$ onto $GMT_{trend}(L)$, with respect to L. The mid-latitude wind stress curl trends signify a poleward shift/intensification of the supergyre circulation[27,33]. The patterns in Figs. 1a and 1b highlight a poleward shift of the atmospheric and oceanic circulation embedded in the positive SAM trends. As warming continues into the future, the resemblance to the SAM pattern strengthens, in a scenario in which increasing CO_2 overwhelms the effect of ozone recovery[25], with the poleward shift becoming even more pronounced.

The tendency of a greater positive SAM trend associated with a stronger positive GMT trend is further highlighted in Fig. 1c, which shows a scatter diagram between trends in GMT and trends in the SAM index. The robust relationship is underscored by a statistically significant correlation of 0.59 between them. These patterns described above are generally of an opposite polarity to the observed in association with interannual variability, as will be discussed below. Hereafter, the observational results are based on 20CRv2 zonal wind stresses[34] and NOAA ERSST.v3b[35,36].

Observed relationship between interannual variability of GMT and circulation fields. Fig. 2 plots one-standard deviation anomalies of zonal winds and sea surface temperatures (SSTs) associated with GMT, Niño3.4, and the SAM. These are obtained through a linear regression using detrended data over the 31 years (1973–2003) of the observed data coverage. We choose this period for illustration because the ENSO-SAM correlation is highest. For clarity, we use a subscript "detrended" to indicate removal of trends in GMT, and "GMT" without the subscript to indicate an inclusion of a long-term trend. Several features emerge. Firstly, an El Niño event is associated with a higher $GMT_{detrended}$ (Fig. 2a) as the tropical ocean releases heat to the atmosphere during an El Niño event. An important feature to note is that a higher $GMT_{detrended}$ is linked to a negative SAM-like pattern in zonal winds (Fig. 2b), with enhanced westerlies in the mid-latitudes.

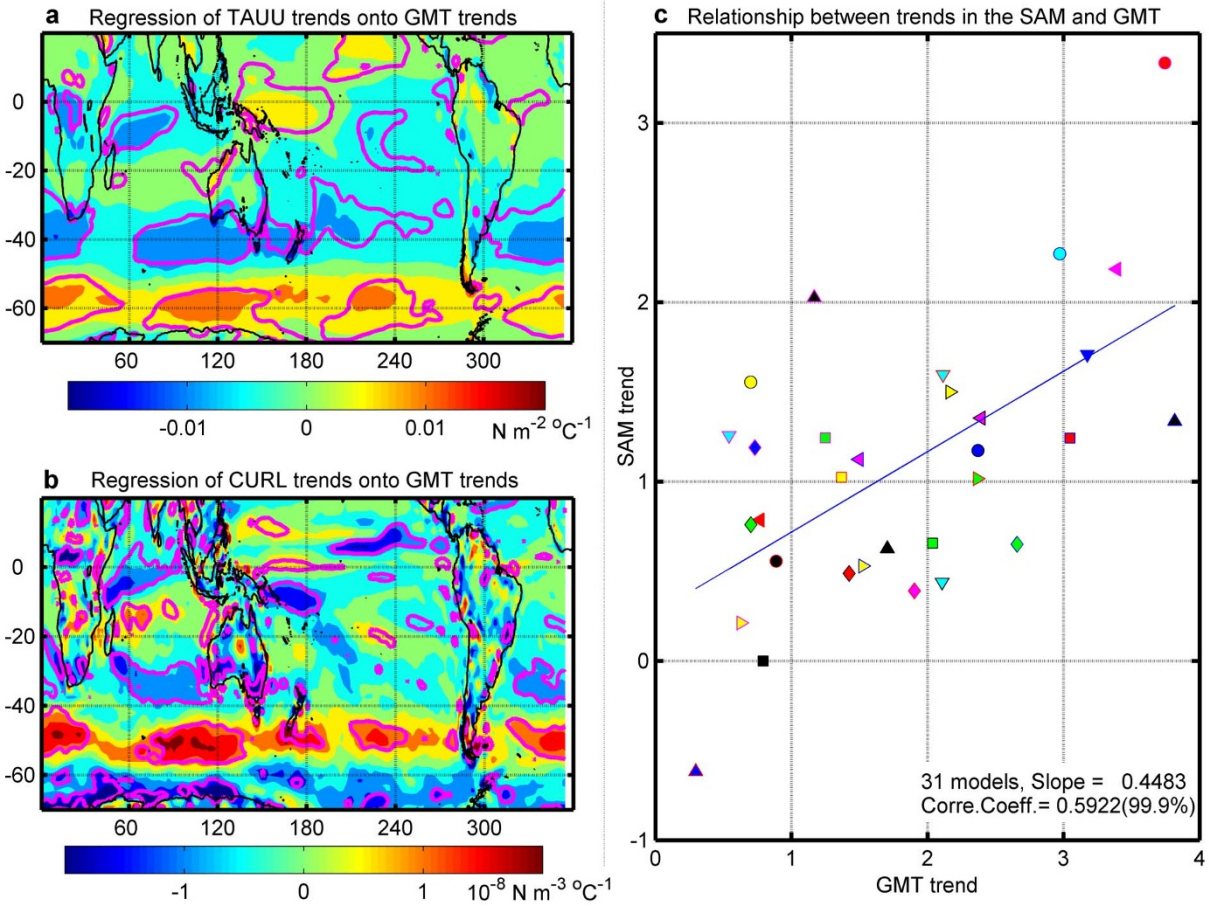

Figure 1 | Inter-model relationships of GMT with circulation fields and the Southern Annular Mode. Map of regression of (a), trends of zonal wind stress field $TAUU_{trend}(x, y, L)$ ($L = 1, 31$, *representing models*) onto *GMT (L) trends*, and (b), trends of wind stress curl ($CURL_{trend}(x, y, L)$) onto *GMT (L) trends*, with respect to models (L), from 14 CMIP3 and 17 CMIP5 models (see Supplementary Table S1 online). Areas within thick contours indicate correlations significant at the 95% confidence level using Student's t test. (c), scatter plot between trends in *SAM (L)* and trends in the *GMT (L)*.

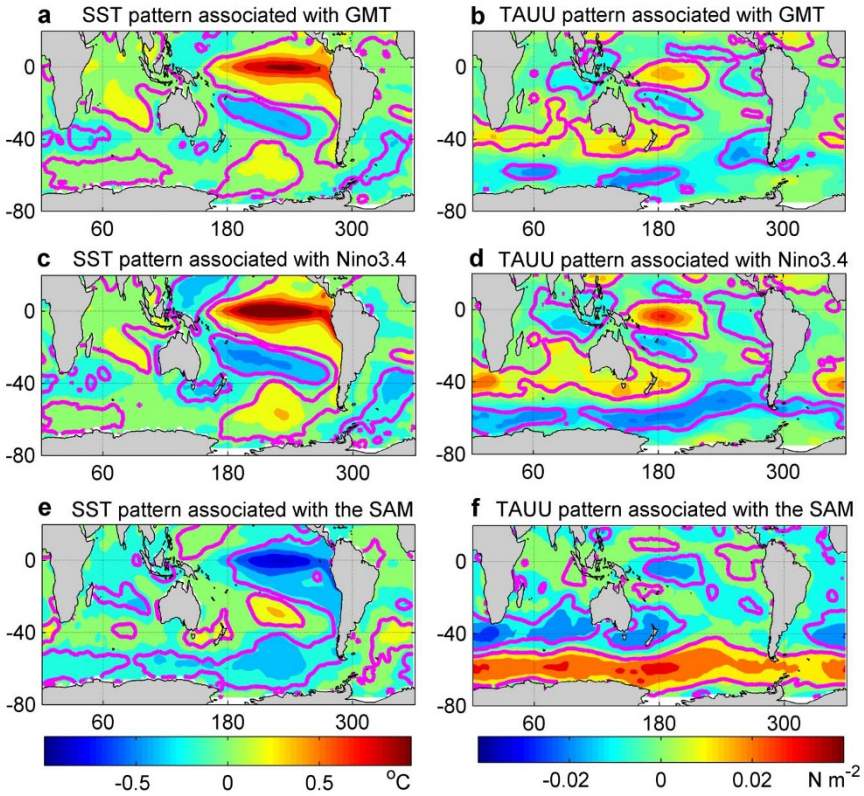

Figure 2 | One standard deviation anomaly patterns of SST and zonal winds over a 31-year period centred at 1988. Shown are associated with GMT (a and b), ENSO (c and d), and the SAM (e and f) using detrended observational data over a 31-year period centred at 1988. The anomalies are calculated by regressing detrended grid-point anomalies onto a detrended index, and then multiplying the one-standard deviation value of the index. Areas confined by the purple contours indicate a statistical significance at the 95% confidence level using Student's *t* test. The left (right) color bar is for the figures in the left (right) column.

Secondly, the SAM-like zonal wind pattern seen in Fig. 2b is almost identical to that associated with an El Niño event (Fig. 2d). Finally, on interannual time scales, a positive SAM is linked to a La Niña, and vice-versa (Figs. 2e and 2f), as revealed and discussed by previous studies[10,11]. The ENSO-SAM relationship means that during an El Niño event there is an increasing $GMT_{detrended}$ associated with both a negative SAM and a tendency for an equatorward shift of the subtropical gyre circulation. This is because the negative SAM features a decreasing mid-latitude wind stress curl and an equatorward shift in the zero-wind stress curl line as indicated by the extratropic positive and mid-latitude negative curl anomalies (see Supplementary Fig. S1 online).

There is no obvious dynamical linkage between $GMT_{detrended}$ and zonal wind variability. A plausible explanation is that this linkage is generated by the common forcing of ENSO: an El Niño event leads to a higher $GMT_{detrended}$ and a negative SAM. This interannual SAM-$GMT_{detrended}$ relationship, however, is opposite to that seen in the inter-model relationship between the long-term SAM trends and GMT trends (Fig. 1) in all respects. For example, on interannual time scales, a higher GMT is associated with decreasing westerlies in high latitudes (Fig. 2b), opposite to the feature of a greater GMT trend associated with trends of enhancing westerlies (Fig. 1a). Is the interannual SAM-$GMT_{detrended}$ relationship stable and robust?

Multidecadal variability of the interannual GMT-SAM relationship. It turns out that the interannual SAM-$GMT_{detrended}$ relationship undergoes considerable fluctuations (**blue**, Fig. 3a) over the 20th century. An evolution of the relationship, together with that of the ENSO-$GMT_{detrended}$ (**red**) and the ENSO-SAM (**green**) is calculated using a 31-year sliding window. Data are linearly detrended within each window before the correlation analysis. To test the robustness of our result, we also use HadISST v.1.1[37] in place of ERSST.v3b[35,36] to generate the equivalent plot to Fig. 3. The result is similar (see Supplementary Fig. S2 online). Overall, the evolution supports the notion that without climate change signals, ENSO simultaneously drives variability of $GMT_{detrended}$ and the SAM, resulting in an ENSO-$GMT_{detrended}$, and ENSO-SAM relationship[10], both stronger than a SAM-$GMT_{detrended}$ relationship when the correlation is negative (comparing **green** and **blue** curve of Fig. 3a). The central feature to emphasize is the strong multidecadal fluctuation of the SAM-$GMT_{detrended}$ relationship. Early in the century (e.g., the 31-year period centred at 1901), the relationships among these climate indicators are similar to that since early 1970s; strong correlations are seen in both periods. Equivalent maps to Fig. 2 for this early period show a strong resemblance (see Supplementary Fig. S3 online). Further, there is a collapse in the SAM-$GMT_{detrended}$ relationship in the decadal period at around 1940 towards what is consistent with the inter-model relationship between GMT trends and the SAM trends (Fig. 1). However, this does not imply a similar mechanism, as we will discuss below.

The SAM-$GMT_{detrended}$ correlation during the 1940 reversal period is generally not statistically significant above the 95% confidence level by Student's *t* test. This is illustrated in Fig. 4, similarly constructed as in Fig. 2. There is no well-defined SAM pattern associated with the $GMT_{detrended}$ (Fig. 4b). During this decadal period, ENSO is generally weaker than during the 31 years of the 1973–2003 period (comparing Fig. 4c with Fig. 2c, see also Supplementary Fig. S4 online). Although still influencing $GMT_{detrended}$, ENSO no longer induces a SAM pattern (Fig. 4d), and the SAM in this period is not coherent with ENSO (Figs. 4e and 4f), as the impact from the weak ENSO is unable to be manifest out of stochastic noises. Thus, the role of ENSO in linking $GMT_{detrended}$ and the SAM, seen at the beginning

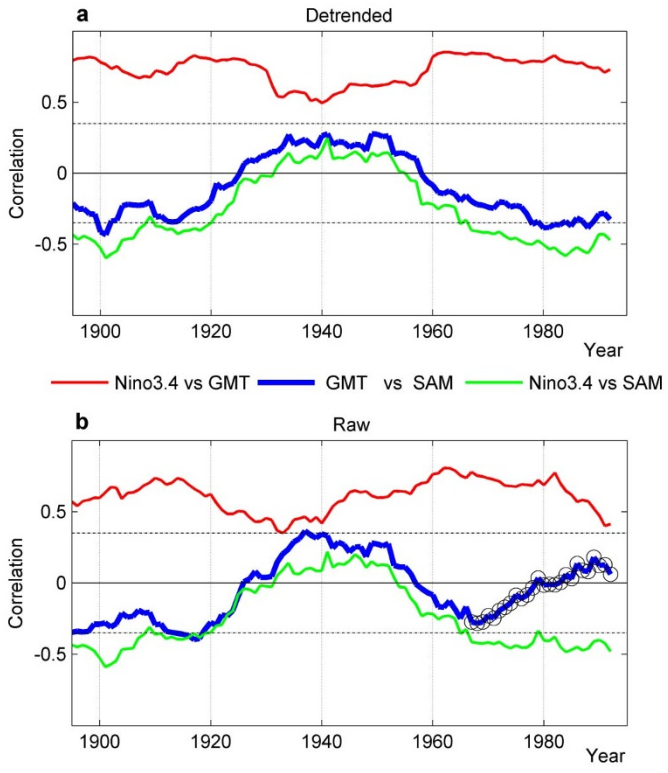

Figure 3 | Evolution of correlations among ENSO (i.e., Niño3.4), GMT, and the SAM in the 20th Century. Evolution of correlation between ENSO and GMT (**red** curve), GMT and the SAM (**blue** curve), and ENSO and the SAM (**green** curve) are shown using, (a), time series linearly detrended within each of a 31-year sliding window, and (b) raw time series. The correlation coefficient required to reach statistical significance at the 95% confidence level by Student's *t* test is indicated by horizontal dashed lines.

of the century and the past decades, collapses. We conclude that the relationship between the $GMT_{detrended}$ and the SAM during the 1940 reversal period is at least partially due to a lack of influence from ENSO, as ENSO variability is weak.

Given that the canonical and Modoki ENSO exert a distinctly different impact in austral summer[38–40], we have replaced Niño3.4 with an El Niño Modoki index (EMI, constructed as in Ref. 41) in an otherwise identical calculation of correlation to that for Fig. 3 (see Supplementary Fig. S5 online). The result shows that the general features are the same as those shown in Fig. 3. For example, the influence of the EMI on the GMT and the influence of the EMI on the SAM are similar, showing a weakening in the period centred at the 1940s. This is in part due to the fact that in this season the EMI and Niño3.4 are highly correlated (the correlation coefficient is 0.57, which is statistically significant at the 99.9% confidence level by Student's *t* test). As described previously[41], correlation of this magnitude is expected, and can be explained by the fact that both types of events occur in the common ground of the tropical Pacific. Thus, our conclusions, with respect to canonical ENSO, on its time-varying relationship with the SAM and the GMT carry over to Modoki ENSO.

We notice that our conclusion regarding this collapse of the SAM-$GMT_{detrended}$ relationship is purely based on available data, which suffer from issues such as data loss during the World War II period, low quality due to different measurement processes[42], and a low coverage of in-situ observations[43]. All these factors can affect the ENSO index. It is not clear how these issues affect our conclusions. Regardless of these issues, the main point is that the relationship between the long-term trend of the SAM and GMT is opposite to the SAM-$GMT_{detrended}$ relationship, which is the major focus of our study.

Impact of global warming on the interannual SAM-GMT relationship. Given that global warming has been occurring over the 20th century, we expect a signature in the evolution of the SAM-GMT relationship beyond the fluctuating ENSO influences on an interdecadal time scale. As discussed in the context of Fig. 1, the relationship between the long-term SAM and GMT trends is opposite to that between the SAM and $GMT_{detrended}$. To this end, we repeat the sliding-window correlation analysis without detrending (Fig. 3**b**), i.e., retaining climate change signals. An indication of an impact on the SAM-$GMT_{detrended}$ relationship by climate change (trends) emerges. During the 31-year period with a weak ENSO (see Supplementary Fig. S4 online), centred at approximately 1938, the trends in the SAM and GMT add to the reversed correlation (comparing **blue** curves in Fig. 3a and b), enabling it to reach a statistically significant value at the 95% confidence level by Student's *t* test. This suggests that climate change might play a part in further weakening the SAM-$GMT_{detrended}$ relationship.

A more prominent signature is recorded in the period since the early 1970s, when data from early 1980 onward are included in the 31-year correlation. During this time the SAM and the GMT have been trending upward strongly; the former is in part due to Antarctic Ozone depletion[23,27,28], and the latter, due to greenhouse warming. The strong coherence between the long-term trends of the SAM and GMT offsets the SAM-$GMT_{detrended}$ negative correlation due to interannual variability. Since the 1980s, ENSO has been rather strong, and the world experiences the 1982/83 and 1997/98 super-El Niño events, the strongest of the century. However, there is no a statistically significant trend in Niño3.4 apart from the well-known climate shift in the mid-1970s. Despite the well-defined SAM pattern associated with the strong ENSO (Fig. 2d) in association with the strong ENSO-SAM correlation (**green**, Fig. 3b), the SAM-GMT correlation weakens (circled **blue** curve, Fig. 3b) once long-term GMT and SAM trends are included; the opposite relationship between long-term SAM and GMT trends to that between SAM-$GMT_{detrended}$ results in a change in correlation from a negative to a positive value, though the positive correlation is not statistically significant. It also means that, the occurrences of the weakening SAM-GMT relationship commencing around 1920 and 1970 are caused by completely different dynamic processes: the former is due to weak ENSO variability with a minimum in the 1940s, whereas the latter is due to an impact from climate change. This recent weakening in the SAM-GMT relationship occurs in spite of strong ENSO variability during this period, which should have strengthened the relationship.

The opposite relationship between the *long-term* SAM and GMT trends and between *interannual* SAM and $GMT_{detrended}$ variability is intriguing in many respects. It provides an example that global warming signals need not project onto existing teleconnections, i.e., between ENSO and the SAM, despite the fact the impact of global warming does cause an upward trend of the SAM. This is a distinct situation, which we believe is a rare one, and has important implications for climate change detection. It means that the association of an upward GMT trend with an upward trend in the SAM occurs despite an opposing relationship from interannual variability. Thus, the emergence of a robust symbiosis of the observed increasing GMT trend and the upward SAM trend in recent decades represents a robust climate change signal that manifests despite the impact of the strong ENSO over the past decades that damps the SAM trend.

Discussion

This study highlights that the interannual relationship between the GMT and the SAM undergoes significant multidecadal fluctuations over the 20th century through their common forcing by ENSO variability. An El Niño increases GMT but also forces a negative SAM,

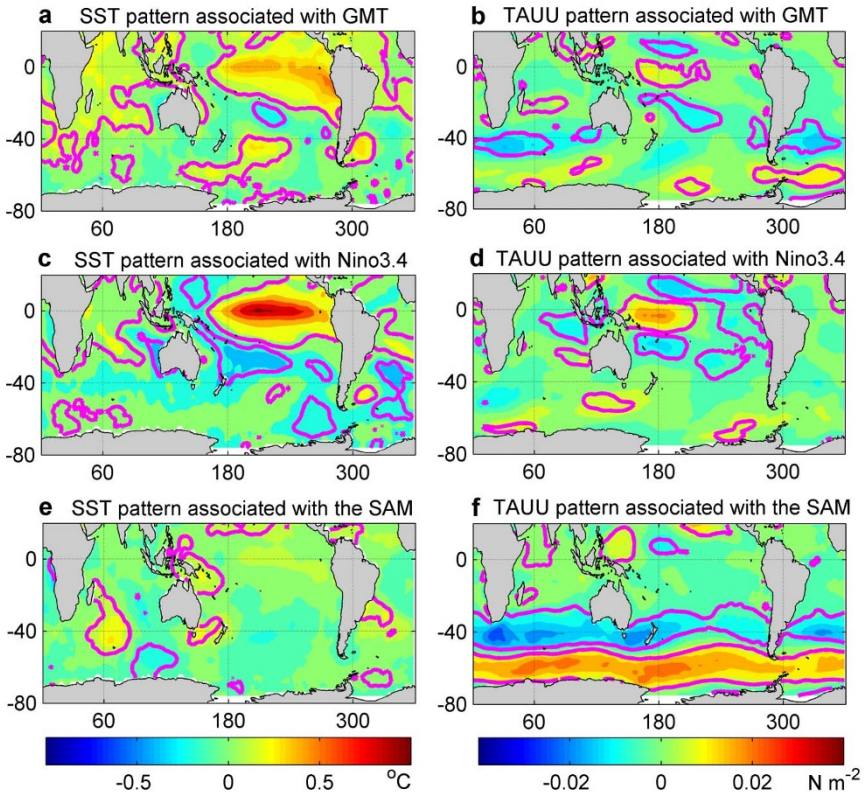

Figure 4 | One standard deviation anomaly patterns of SST and zonal winds over a 31-year period centred at 1940. Shown are associated with GMT (a and b), ENSO (c and d), and the SAM (e and f) using detrended observational data over a 31-year period centred at 1940. The anomalies are calculated by regressing detrended grid-point anomalies onto a detrended index, and then multiplying the one-standard deviation value of the index. Areas confined by the purple contours indicate a statistical significance at the 95% confidence level using Student's *t* test. The left (right) color bar is for the figures in the left (right) column.

leading to a GMT-SAM negative correlation. This negative correlation collapses, even reverses, during the 31-year period centred at the 1940s and during the period since the early 1970s when raw anomalies are used. However, these two periods of reversal are caused by different dynamics. During the 1940s reversal period ENSO is weak and, although still influencing GMT, does not induce a SAM pattern. Since the late 1970s, the negative correlation collapses despite the strong ENSO-SAM relationship associated with the strong ENSO over the period. We show that this collapse is triggered by a global warming-induced trend in GMT and the SAM: an increasing GMT trend is associated with an upward SAM trend, a feature also seen in the inter-model statistics using CMIP3 and CMIP5 models.

This study also shows that climate change signals can emerge against an opposing property of interannual variability. In such a situation, the emerging linkage of the upward SAM trend with an increasing GMT trend, despite a suppressing effect from the recent strong interannual SAM-ENSO relationship, highlights the robustness of the climate change signals in the Southern Hemisphere. This will be particularly useful for climate change detection using climate models. It suggests that realistic simulations of the intensity of ENSO and the SAM, and their relationship will have a direct relevance for climate change detection and climate projection.

Methods

Data. Wind stress data from NOAA 20CRv2 (20th-Century Reanalysis, Version 2), which provide a comprehensive global atmospheric circulation data set spanning from 1870 to 2010[34], are used to construct an austral summer SAM index over the 20th century. This is carried out by applying an empirical orthogonal function (EOF) analysis to austral summer zonal winds, in the domain of 20°S–70°S. We define a SAM index as the time series of the first EOF. The index has a correlation with the observation-based SAM index from *Marshall*[18] of 0.93 over the period since 1958, statistically significant at the 99.9% confidence level by Student's *t* test (see Supplementary Fig. S6 online). NOAA Extended Reconstructed SST version 3b (ERSST.v3b), generated using in situ SST data and improved statistical methods to allow stable reconstruction using sparse data[35,36], is deployed to construct an ENSO index (Niño3.4) and SST anomaly pattern associated with the SAM and Niño3.4. To test the robustness of our results, we use the Met Office Hadley Centre's SST data set (HadISST) v.1.1[37] in place of ERSST. HadISST v.1.1 includes in situ sea surface observations and satellite derived estimates at the sea surface, the SST bucket corrections have been applied to gridded fields from 1870 through 1941, and a blend of satellite AVHRR and observations are used in the modern periods.

Model simulations. To illustrate that a greater GMT trend tends to be associated with a greater SAM trend, we use the SST and wind stress data from the IPCC Special Report on Emission Scenario (SRES) A2 simulations submitted to coupled model intercomparison phase 3 (CMIP3 SRESA2, 14 models)[31], in which CO_2 concentration reaches about 840 ppm at the end of the 21st century and the radiative forcing increases by 7 W/m^2. We also use these variables from the Representative Concentration Pathways (RCP) 8.5 simulations submitted to coupled model intercomparison phase 5 (CMIP5 RCP8.5, 17 models)[32], which is characterized by a rising radiative forcing pathway leading to 8.5 W/m^2 (and about 940 ppm of CO_2) by 2100 (for an identification of models, see Supplementary Table S1 online). Although multiple realizations may exist for an individual model, we only use the first to ensure that all models are equally represented. For the model data, we derive SAM index as described above.

Seasonality. All calculations in this paper are based on data in the austral summer (December, January, and February, or DJF). In this season, the observed SAM trend is rather pronounced and ENSO peaks.

Graphic software. All maps and plots were produced using licensed MATLAB.

1. Limpasuvan, V. & Hartmann, D. L. Eddies and the annular modes of climate variability. *Geophys. Res. Lett.* **26**, 3133–3136 (1999).
2. Thompson, D. W. J. & Wallace, J. M. Annular modes in the extratropical circulation. Part I: Month-to-month variability. *J. Clim.* **13**, 1000–1016 (2000).
3. Rogers, J. C. & van Loon, H. Spatial variability of sea level pressure and 500 mb height anomalies over the Southern Hemisphere. *Mon. Wea. Rev.* **110**, 1375–1392 (1982).

4. Kidson, J. W. Indices of the Southern Hemisphere zonal wind. *J. Clim.* **1**, 183–194 (1988).
5. Hartmann, D. L. & Lo, F. Wave-driven zonal flow vacillation in the Southern Hemisphere. *J. Atmos. Sci.* **55**, 1303–1315 (1998).
6. Lorenz, D. J. & Hartmann, D. L. Eddy–zonal flow feedback in the Southern Hemisphere. *J. Atmos. Sci.* **58**, 3312–3327 (2001).
7. Seager, R., Harnik, N., Kushnir, Y., Robinson, W. & Miller, J. Mechanisms for hemispherically symmetric climate variability. *J. Clim.* **16**, 2960–2978 (2003).
8. Carvalho, L. M. V., Jones, C. & Ambrizzi, T. Opposite phases of the Antarctic Oscillation and relationships with intraseasonal to interannual activity in the tropics during the austral summer. *J. Clim.* **18**, 702–718 (2005).
9. Codron, F. Relation between annular modes & the mean state: Southern Hemisphere summer. *J. Clim.* **18**, 320–330 (2005).
10. L'Heureux, M. L. & Thompson, W. J. Observed relationships between the El Niño–Southern Oscillation and the extratropical zonal-mean circulation. *J. Clim.* **19**, 276–287 (2006).
11. Fogt, R. L. & Bromwich, D. H. Decadal variability of the ENSO teleconnection to the high-latitude South Pacific governed by coupling with the southern annular mode. *J. Clim.* **19**, 979–997 (2006).
12. Ciasto, L. M. & Thompson, D. W. J. Observations of large scale ocean–atmosphere interaction in the Southern Hemisphere. *J. Clim.* **21**, 1244–1259 (2008).
13. Fogt, R. L., Bromwich, D. H. & Hines, K. M. Understanding the SAM influence on the South Pacific ENSO Teleconnection. *Climate Dynamics* **36**, 7–8, 1555–1576 (2010).
14. Pohl, B., Fauchereau, N., Reason, C. J. C. & Rouault, M. Relationships between the Antarctic Oscillation, the Madden–Julian Oscillation, and ENSO, and Consequences for Rainfall Analysis. *J. Clim.* **23**, 238–254 (2010).
15. Gong, T., Feldstein, S. B. & Luo, D. The impact of ENSO on wave breaking and Southern annular mode events. *J. Atmos. Sci.* **67**, 2854–2870 (2010).
16. Cai, W., Sullivan, A. & Cowan, T. Interactions of ENSO, the IOD, and the SAM in CMIP3 Models. *J. Clim.* **24**, 1688–1704 (2011).
17. Ding, Q., Steig, E. J., Battisti, D. S. & Wallace, J. M. Influence of the Tropics on the Southern Annular Mode. *J. Clim.* **25**, 6330–6348 (2012).
18. Marshall, G. J. Trends in the Southern Annular Mode from observations and reanalyses. *J. Clim.* **16**, 4134–4143 (2003).
19. Fyfe, J. C., Boer, G. J. & Flato, G. M. The Artic and Antarctic Oscillations and their projected changes under global warming. *Geophys. Res. Lett.* **26**, 1601–1604 (1999).
20. Kushner, P. J., Held, I. M. & Delworth, T. L. Southern Hemisphere atmospheric circulation response to global warming. *J. Clim.* **14**, 2238–2249 (2001).
21. Cai, W., Whetton, P. H. & Karoly, D. J. The response of the Antarctic Oscillation to increasing and stabilized atmospheric CO_2. *J. Clim.* **16**, 1525–1538 (2003).
22. Lee, S. & Feldstein, S. B. Detecting Ozone- and Greenhouse Gas-Driven Wind Trends with Observational Data. *Science* **339**, 563 (2013).
23. Gillett, N. P. & Thompson, D. W. J. Simulation of recent Southern Hemisphere climate change. *Science* **302**, 273–275 (2003).
24. Arblaster, J. M. & Meehl, G. A. Contributions of external forcings to Southern Annular Mode trends. *J. Clim.* **19**, 2896–2905 (2006).
25. Arblaster, J. M., Meehl, G. A. & Karoly, D. J. Future climate change in the Southern Hemisphere: Competing effects of ozone and greenhouse gases. *Geophys. Res. Lett.* **38**, L02701 (2011).
26. Cai, W., Shi, G., Cowan, T., Bi, D. & Ribbe, J. The response of the southern annular mode, the east Australian Current, and the southern midlatitude ocean circulation to global warming. *Geophys. Res. Lett.* **32**, L23706 (2005).
27. Cai, W. & Cowan, T. Trends in Southern Hemisphere Circulation in IPCC AR4 Models over 1950–99: Ozone Depletion versus Greenhouse Forcing. *J. Clim.* **20**, 681–693 (2007).
28. Thompson, D. W. J. & Solomon, S. Interpretation of recent Southern Hemisphere climate change. *Science* **296**, 895–899 (2002).
29. Marshall, G. J. & Connolley, W. M. Effect of changing Southern Hemisphere winter sea surface temperatures on Southern Annular Mode strength. *Geophys. Res. Lett.* **33**, L17717 (2006).
30. Clarke, G. K. C. *et al*. Physical climate processes and feedbacks. *Climate Change 2001: The Scientific Basis.* Houghton, J. T. *et al*. Eds. Cambridge University Press 417–470 (2001).
31. Meehl, G. *et al*. The WCRP CMIP3 multimodel Dataset: A New Era in Climate Change Research. *Bull. Amer. Meteor. Soc.* **88**, 1383–1394 (2007).
32. Taylor, K. E., Stouffer, R. J. & Taylor, K. E., Stouffer, R. J. & Meehl, G. A. An Overview of CMIP5 and the experiment design. *Bull. Amer. Meteor. Soc.* **93**, 485–498 (2012).
33. Cai, W. Antarctic ozone depletion causes an intensification of the Southern Ocean super-gyre circulation. *Geophys. Res. Lett.* **33**, L03712 (2006).
34. Compo, G. P. *et al*. The Twentieth Century Reanalysis Project. *Q. J. Roy. Met. Soc.* **137**, 1–28 (2011).
35. Smith, T. M., Reynolds, R. W., Peterson, T. C. & Lawrimore, J. Improvements to NOAA's Historical Merged Land-Ocean Surface Temperature Analysis (1880-2006). *J. Clim.* **21**, 2283–2296 (2008).
36. Xue, Y., Smith, T. M. & Reynolds, R. W. Interdecadal changes of 30-Yr SST Normals during 1871–2000. *J. Clim.* **16**, 1601–1612 (2003).
37. Rayner, N. A. *et al*. Global analyses of sea surface temperature, sea ice, and night marine air temperature since the late nineteenth century. *J. Geophys. Res.* **108**(D14), 4407 (2003).
38. Weng, H., Behera, S. K. & Yamagata, T. Anomalous winter climate conditions in the Pacific rim during recent El Niño Modoki and El Niño events. *Clim. Dyn.* **32**, 663–674 (2009).
39. Yeh, S. *et al*. El Niño in a changing climate. *Nature* **461**, 511–514 (2009).
40. Taschetto, A. S., Gupta, A. S., Hendon, H. H., Ummenhofer, C. C. & England, M. H. The Contribution of Indian Ocean Sea Surface Temperature Anomalies on Australian Summer Rainfall during El Niño Events. *J. Clim.* **24**, 3734–3747 (2011).
41. Ashok, K. *et al*. El Niño Modoki and its possible teleconnection. *J. Geophys. Res.* **112**, C11007 (2007).
42. Thompson, D. W. J., Kennedy, J. J., Wallace, J. M. & Jones, P. D. A large discontinuity in the mid-twentieth century in observed global-mean surface temperature. *Nature* **453**, 646–650 (2008).
43. Deser, C., Alexander, M. A., Xie, S. & Phillips, A. S. Sea Surface Temperature Variability: Patterns and Mechanisms. *Annu. Rev. Mar. Sci.* **2**, 115–143 (2010).

Acknowledgements

This work was carried out while Guojian Wang was a Ph. D student of Ocean University of China, supported by a scholarship from China Scholarship Council, which enabled his visit to CSIRO Marine and Atmospheric Research. Wenju Cai is supported by the Australian Climate Change Science Programme. We thank Ariaan Purich and WonMoo Kim for a review before submission.

Author contributions

G.W. and W.C. conceived and designed the analysis. G.W. conducted the analysis. W.C. and G.W. wrote the manuscript together.

Additional information

Supplementary information accompanies this paper at http://www.nature.com/scientificreports

Competing financial interests: The authors declare no competing financial interests.

How to cite this article: Wang, G. & Cai, W. Climate-change impact on the 20th-century relationship between the Southern Annular Mode and global mean temperature. *Sci. Rep.* **3**, 2039; DOI:10.1038/srep02039 (2013).